Misfit strain driven cation inter-diffusion across an epitaxial multiferroic thin film interface

P. S. Sankara Rama Krishnan, Anna N. Morozovska, Eugene A. Eliseev, Quentin M. Ramasse, Demie Kepaptsoglou, Wen-I. Liang, Ying-Hao Chu, Paul Munroe, and V. Nagarajan

Citation: Journal of Applied Physics **115**, 054103 (2014); doi: 10.1063/1.4862556
View online: http://dx.doi.org/10.1063/1.4862556
View Table of Contents: http://scitation.aip.org/content/aip/journal/jap/115/5?ver=pdfcov
Published by the AIP Publishing

Misfit strain driven cation inter-diffusion across an epitaxial multiferroic thin film interface

P. S. Sankara Rama Krishnan,[1] Anna N. Morozovska,[2] Eugene A. Eliseev,[2] Quentin M. Ramasse,[3] Demie Kepaptsoglou,[3] Wen-I. Liang,[4] Ying-Hao Chu,[4] Paul Munroe,[1] and V. Nagarajan[1]
[1]*School of Materials Science and Engineering, The University of New South Wales, Sydney, New South Wales 2052, Australia*
[2]*Institute of Physics, Institute of Material Sciences, NAS of Ukraine, 03028 Kiev, Ukraine*
[3]*SuperSTEM laboratory, SciTech Daresbury, Daresbury WA4 4AD, United Kingdom*
[4]*Department of Materials Science and Engineering, National Chiao Tung University, Hsinchu 30010, Taiwan*

(Received 31 October 2013; accepted 6 January 2014; published online 4 February 2014)

Cation intermixing at functional oxide interfaces remains a highly controversial area directly relevant to interface-driven nanoelectronic device properties. Here, we systematically explore the cation intermixing in epitaxial (001) oriented multiferroic bismuth ferrite (BFO) grown on a (001) lanthanum aluminate (LAO) substrate. Aberration corrected dedicated scanning transmission electron microscopy and electron energy loss spectroscopy reveal that the interface is not chemically sharp, but with an intermixing of ~2 nm. The driving force for this process is identified as misfit-driven elastic strain. Landau-Ginzburg-Devonshire-based phenomenological theory was combined with the Sheldon and Shenoy formula in order to understand the influence of boundary conditions and depolarizing fields arising from misfit strain between the LAO substrate and BFO film. The theory predicts the presence of a strong potential gradient at the interface, which decays on moving into the bulk of the film. This potential gradient is significant enough to drive the cation migration across the interface, thereby mitigating the misfit strain. Our results offer new insights on how chemical roughening at oxide interfaces can be effective in stabilizing the structural integrity of the interface without the need for misfit dislocations. These findings offer a general formalism for understanding cation intermixing at highly strained oxide interfaces that are used in nanoelectronic devices. © *2014 AIP Publishing LLC*. [http://dx.doi.org/10.1063/1.4862556]

I. INTRODUCTION

The use of substrate-induced epitaxial strain to modulate physical properties has been a powerful and effective method to realise new functional behaviour in oxide heterostructures.[1–3] Recently, Zeches *et al.* have demonstrated that a morphotropic phase boundary comprising a "mixed-phase" can be induced in (001) epitaxial bismuth ferrite (BFO) thin films by careful tuning of the applied epitaxial strain.[4] The so-called "mixed-phase BFO," comprises a nanoscale mixture of tetragonal (T-like) and rhombohedral (R-like) phases and is obtained by depositing (001) BFO on a substrate which induces in-plane compressive strains, such as a (001) lanthanum aluminate (LAO). Mixed phase BFO has garnered significant technological interest as it possess a much larger electromechanical coefficient compared with the individual R and T phases,[5] electromechanical strains as large as 5% for fields greater than 1000 kV/cm are attributed to the interphase (R-T) boundary motion.[6,7] Further He *et al.* demonstrated that the underlying strain, due to the co-existence of T and R mixed phases can lead to enhanced spontaneous magnetic moment and this is switchable only by the electric field.[8,9] An enhanced spontaneous polarization of ~150 μC/cm^2 was reported for the pure T-rich BFO film.[10] These additional functionalities have made the mixed phase BFO thin film system an attractive candidate for lead-free multiferroic device platforms, where the observed control of magnetic moments by the electric field and very high spontaneous polarization have opened new avenues for realising nanoelectronic devices.

One of the most intriguing characteristics of these mixed-phase BFO heterostructures is the lack of periodic misfit dislocations (MDs) at the BFO-substrate interface. LAO imposes a 4.5% compressive strain on the BFO layer. In the context of typical heteroepitaxy conditions, this is an enormous value. Typically, such large strains would be relaxed by the formation of MDs at the interfaces beyond certain levels of critical thicknesses, known as the Mathews-Blakeslee criteria for MD formation.[11–14] Yet this does not occur (or at least has never been reported) for mixed phase BFO thin films. From a device perspective, it is imperative to understand this as it has been shown that the strain field associated with defects at an oxide interface can propagate several nanometres into the material bulk and drastically degrade device performance.[15]

Prima-facie, the spontaneous phase separation of BFO into the T- and R-like phases can be considered to be the strain-relief mechanism accommodating this epitaxial compressive misfit strain.[16,17] One could argue that the very close in-plane matching of the T-phase (typically it has in-plane lattice parameter of 0.377 nm) with LAO should not generate any misfit dislocations. However, there are two key inconsistencies with this line of thought. Firstly, such phase transformations occur only once the film begins to cool down below the Curie temperature. On the other hand, misfit

dislocations are expected to form at the growth temperatures and hence should ordinarily be the first response mechanism by the thin film heterostructure to relax the induced epitaxial strain. The phase separation model is thus not able to explain why mixed phase BFO thin films remains unaffected without any dislocation formation even at much larger thicknesses (~100 nm). Secondly, the R- (or R′ as defined by some reports) phase still has a very large mismatch with the underlying substrate. Therefore, it is very likely that the mechanism of compensation for such a large misfit strain at the interface is an alternate defect or chemical transport mechanism that has not been considered yet. This information is critical, as it is now well-known that both the physical properties and the local chemistry at defect cores which can be substantially different from the bulk parent lattice for perovskite ferroics, have large bearing on the ferroelectric polarization required for the nanoelectronic device.[18–21]

In functional oxide heterostructure interfaces, phenomena, such as cation mobility across the interfaces[19,22–24] and interfacial misfit strains and its associated octahedral tilts,[25–27] are very important since they can significantly alter the interfaces, as well as the bulk physical and chemical behaviours.[28–30] Furthermore, the presence of interfacial defects, such as oxygen vacancies, and chemical diffusion arising due to misfit strain, can directly influence the ferroelectric order parameters.[31]

It is necessary to know if these mechanisms are applicable to the LAO-BFO system. The high level of structural integrity achieved could be a consequence of chemically driven strain-relaxation mechanisms at the interface, such as chemical diffusion, interfacial charge imbalances, built-in fields, and vacancy formation. Furthermore, the effect on the stability of these interfaces due to high temperature kinetics issues, such as cation volatility, surface roughening, and reconstruction during growth, still needs to be understood. Hence, a detailed investigation into interface chemistry and its associated long-range field effects on the structural integrity and chemical variation across this highly strained oxide interface becomes necessary.

In this study, we report atomically resolved electron energy loss spectroscopy (EELS) chemical information which reveals the intermixing of cations across the LAO-BFO interface over a length of ~2 nm. Theoretical calculations based on parameters, such as misfit strain, spatial distribution of defects concentration, and interfacial built-in potential, indicate the presence of a strong potential gradient at the interface, which decays on moving into the bulk of the film. The misfit strain, and other interfacial effects, induces a potential gradient which drives the cation migration across the interface, thereby bringing in the additional structural stability to the interface.

II. MATERIALS AND METHODS

Epitaxial mixed phase BFO was deposited on a (001) LAO substrate using pulsed laser deposition (PLD) with a krypton fluoride (KrF) 248 nm laser. LAO substrate used in this study is a commercial single crystal substrate with purity of 99.99% and one-side polished. Prior to deposition, substrate was ultrasonically cleaned for 5 min in acetone and then blown to remove residue on substrate by nitrogen gas. The laser energy density was ~4–5 J cm^{-2} with a repetition rate of 10 Hz. The BFO film was deposited at 750 °C and an oxygen pressure of 100 mTorr. A BFO target with a 7.3 g cm^{-3} density and 99.99% purity was used. After the deposition, the heterostructure was cooled at 20 °C min^{-1}. The deposition parameters were controlled to yield a BFO thin film of ~50 nm thickness.

X-ray diffraction (XRD) was carried out using a Pan Analytical MRD, in theta-2theta mode for a scan angle ranging between 15° and 90°. Copper K-alpha radiation with a wavelength of 0.154 nm was used as the X-ray source. Atomic force microscopy (AFM) studies were carried out using a Multimode—AFM (Digital Instruments).

Cross-sectional transmission electron microscopy samples were prepared using conventional tripod grinding followed by room temperature ion beam thinning using PIPS.[32] Atomic resolution Z-contrast scanning transmission electron microscopy (STEM) images were obtained using a dedicated aberration corrected STEM (Nion UltraSTEM100) operated at 100 kV, equipped with a cold field emission electron source. Atomic resolution STEM-EELS studies were carried out by acquiring line scans across the LAO-BFO interface (moving the electron probe serially across the interface and recording a spectrum at each point) using a Gatan Enfina spectrometer. Although the native resolution of the instrument is ~0.35 eV, the spectrometer energy dispersion was set up to observe simultaneously the O-K, Fe-$L_{2,3}$, and La-$M_{4,5}$ edges, resulting in an effective resolution of ~0.80 eV (estimated by the full width at half-maximum of the zero loss peak), limited by the detector point spread function. The convergence and collection semi-angles were 29 mrad and 36 mrad, respectively.

III. RESULTS

A. Basic structural data of BFO-LAO film

The XRD data for the LAO-mixed phase BFO heterostructure is shown in Figure 1(a). Three distinct peaks characteristic of (001), (002), and (003) LAO planes were observed at 2 theta values ~23.7°, 47.8°, and 75.1°, respectively. The (001), (002), and (003) planes for T-like BFO were characterized by peaks at ~19.1°, 38.5°, and 59.5°, respectively. The peaks at ~22.3° and 45.5° represent the (001) and (002) planes for R-like BFO, respectively.[4,33] There are no additional peaks observed thereby confirming the epitaxial nature of the LAO-BFO film.

The topography of the BFO film can be observed from Figure 1(b) and it consists of two distinct features (a) the featureless region from the pure T-phase and (b) local striated regions arising from the mixed T and R phases. The striated regions are in two orientations (shown in two circles, blue and orange) that are almost perpendicular to each other. This confirms that a mixed phase with a stable minimum energy was achieved.[6,34]

The out of plane lattice parameter for the T-like phase, based on the reciprocal space mapping (RSM) data shown in Figure 1(c), is measured to be 0.464 nm, whilst it is 0.416 for

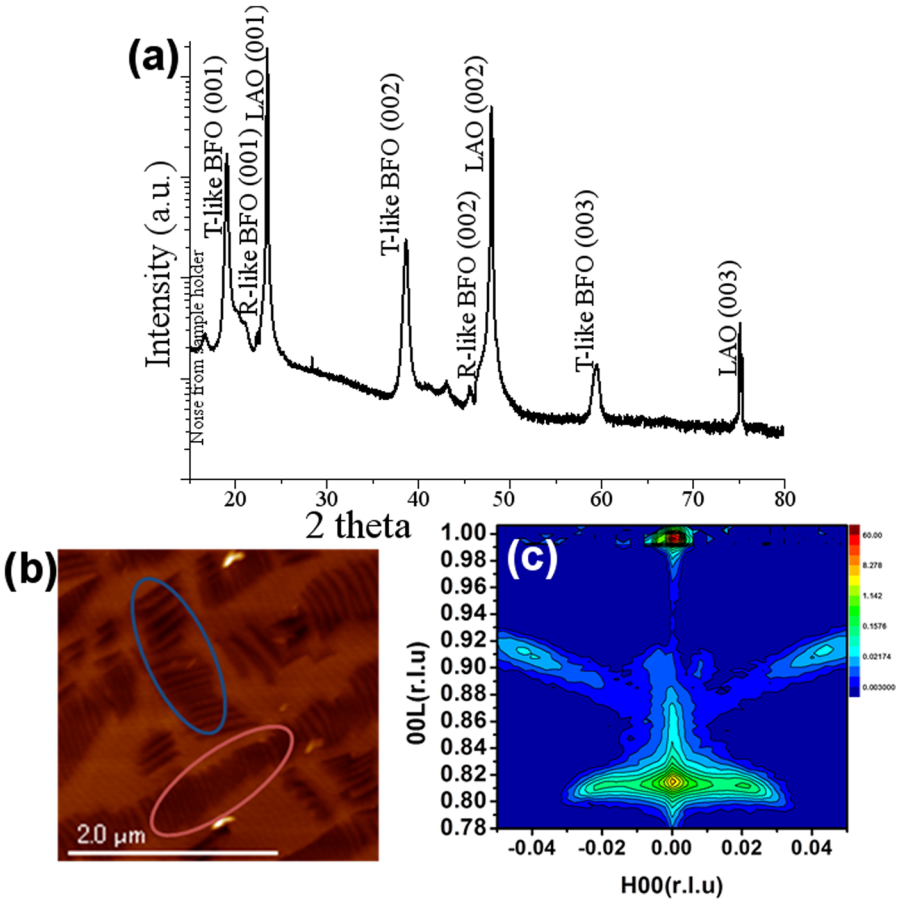

FIG. 1. (a) XRD spectra confirming the epitaxial nature of the film and the presence of mixed phase (R-T like phases) BFO, (b) AFM image showing the topography confirming the formation of mixed phase BFO. The observation of plain and striated regions confirms the co-existence of T phase and mixed phases (R and T like), respectively, and (c) the RSM of LAO-BFO sample.

the R-like phase. The measured values for the T-like phase are in very close agreement with those reported for single-phase T-like films.[10,35] This means the R-T phase separation does not relax the dimensions of the T-phase. In fact, recent studies on the phase evolution of this system reveal that it is only when film thicknesses reach as high as 350 nm does the T-phase entirely disappear.[36] An epitaxial strain of the order of 4.5% cannot be sustained to such thicknesses (despite well-known barriers to dislocation formation in complex oxide thin film heterostructures).[37] This strongly hints to an alternative strain relaxation mechanism driven by the peculiarities of the interface between mixed phase BFO and the underlying LAO substrate.

B. High-resolution STEM results

STEM high angle annular dark field (HAADF) images of the LAO-BFO interface are shown in Figure 2(a) and confirm the thickness of the BFO layer to be ~50 nm. The atomic resolution image of the interface shown in Figure 2(b) reveals that while the interface is dislocation-free, there is clearly some distortion of the atomic planes due to the lattice mismatch. Furthermore, the change of image contrast between the LAO and BFO sides is not abrupt. The contrast in HAADF images depends approximately on the average atomic weight Z of the observed material as $\sim Z^n$ ($n = 1.7$–2), and this technique is thus often referred to as Z-contrast imaging.[38–40] In the case of an atomically sharp interface between layers containing elements of different atomic weights, the contrast change should thus be reasonably abrupt, although this situation, is of course, often complicated by thickness and probe channelling effects so that the direct interpretation of image contrast in terms of interface sharpness is often not straightforward.[41] We note, however, that in almost identical conditions (sample growth, preparation and thickness as well as microscope observation conditions), abrupt image intensity changes were observed for the case of the closer matched $La_{0.7}Sr_{0.3}MnO_3/BiFeO_3$ interface, which was determined to be chemically sharp.[42] In the LAO-BFO interface image shown in Figure 2(b), a region marked with a white dotted line acts as a guide to the

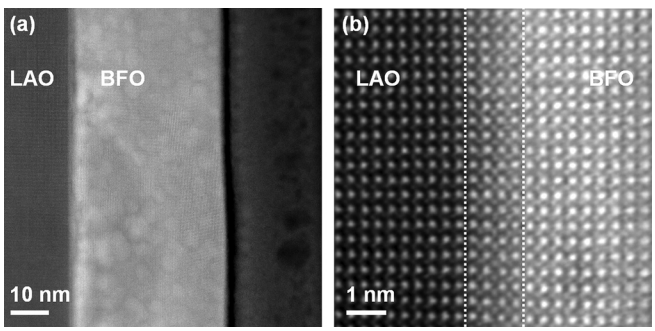

FIG. 2. (a) STEM HAADF image showing the ~50 nm thick BFO film grown on a LAO substrate. (b) High resolution STEM HAADF image of the LAO/BFO interface, showing a diffuse contrast across the interface (dotted white lines are added as a guide to the eye), suggesting some chemical inter-diffusion. The image was sheared by 6.5° to correct for scan non-orthogonality, and filtered using a low-pass Butterworth filter for clarity.

eye and clearly displays an intermediate contrast level raising the possibility of cation intermixing across the interface.

In order to understand the chemical profile across the interface, a number of atomic resolution electron energy loss (EEL) linescans were acquired by moving the STEM probe serially across the LAO-BFO interface and recording an EEL spectrum at each point. Figure 3(b) shows examples of EEL spectra for the O-K, Fe-$L_{2,3}$, and La-$M_{4,5}$ edges from a linescan recorded along the direction schematically indicated by the red arrow in Figure 3(a). The example spectra, acquired from the LAO substrate into BFO film are labelled 1–8, corresponding to the positions marked 1–8 on Figure 3(a). Moving from the LAO substrate towards the BFO, the La-$M_{4,5}$ peak at 832 eV, indicative of the presence of La, does not disappear abruptly, weakening gradually instead with some La signal still visible at spectrum 7. Similarly, although visually the interface would appear to be around spectrum 5, the Fe $L_{2,3}$ edge at 708 eV is already visible in spectrum 4, i.e., in the region of "intermediate" contrast. The chemical profile of Figure 3(c) shows periodic oscillations corresponding to the various lattice planes of the structure and was obtained by integrating the Fe and La signals over a 50 eV window above the edge onsets (after background subtraction using a power law fit). It confirms the presence of a region of mixed chemistry containing both Fe and La, over a distance of 1.5–2.5 nm or 3–5 perovskite unit cells along the linescan. As for Z-contrast images, the interpretation of EELS data in terms of interface sharpness is not straightforward.[19,24] Effects, such as the intrinsic delocalisation of the signal, collection conditions, or probe de-channelling and sample thickness, must thus be carefully considered before drawing any conclusion.[43,44] Here, several factors may contribute to some La and Fe signal being observed slightly away from the apparent interface: the La M edge is typically quite delocalised,[45] although a large collection angle (36 mrad semi-angle for a 29 mrad convergence semi-angle) was, however, used to minimize delocalisation effects; the sample, while relatively thin (the estimated thickness using the log-ratio method is ~35 nm), did not allow a regime where the electron probe remained within a single atomic column. However, using extremely similar experimental conditions, it was possible to clearly distinguish between narrower chemical inter-diffusion profiles across related complex oxide heterojunctions.[27,42,46,47] Taken together, the observation of mixed cation signal over 3–5 unit cells and the very gradual Z-contrast change across the interface in spite of favourable observation conditions, provide strong evidence for the presence of pronounced cation inter-diffusion across the LAO/BFO interface.

The driving force behind such interdiffusion remains unclear: with no observable defects or dislocations providing pathways for cation migration, it was hypothesized that the imposed large misfit strain may play an important role.

C. Development of thermodynamic theory

In order to understand the influence of the misfit strain on cation migration, previously developed phenomenological theory based on Landau-Ginzburg-Devonshire (LGD) formalism[48] was combined with models of Stephenson and Highland,[49] and Sheldon and Shenoy[28] to calculate the charged defects spatial distribution in thermodynamic equilibrium. The cation profile in a BFO film of thickness h clamped to a thick rigid LAO substrate is shown schematically in Figure 4(a). The axis x_3 is perpendicular to the BFO film surface. Calculation details are explained in Appendix A of supplementary material.[50] The approximate analytical expression for the cation concentration $N(x_3)$ across the LAO-BFO interface was derived as follows:

$$N(x_3) \propto N^0 \exp\left(\frac{W\left(u_m - Q_{12}\bar{P}_3^2\right)}{(s_{11}+s_{12})k_BT} - \frac{eZ\varphi(x_3)}{k_BT}\right), \quad (1)$$

where N^0 is the equilibrium bulk concentration of donors, W is the Vegard strain coefficient,[51–53] u_m is the film-substrate misfit strain, Q_{12} is the electrostriction tensor coefficient, P_3 is the out-of-plane polarization component, s_{ij} are elastic compliances, Z is the cation effective charge in the units of the electron charge e; φ is the built-in electric potential, and T is the absolute temperature.

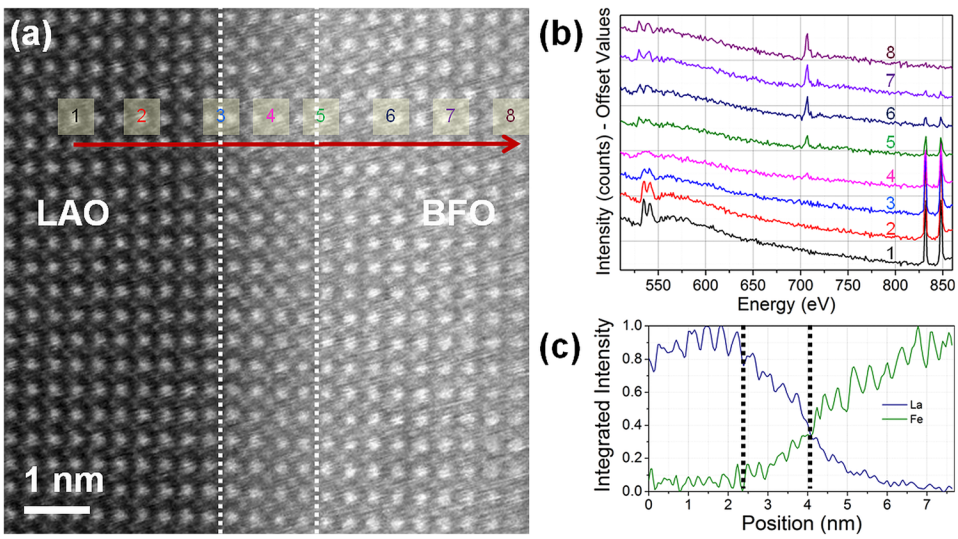

FIG. 3. (a) STEM-EELS survey image showing the path of the EELS line scan (red arrow) acquired across the LAO-BFO interface. The image was sheared by 6.5° to correct for scan non-orthogonality, but otherwise unprocessed. (b) Raw spectra (averaged over 3 adjacent data points to improve S/N) extracted from the STEM-EELS linescan at the position indicated on (a), showing the simultaneous presence of La and Fe over an extended region. (c) Chemical profiles for La and Fe across the interface, obtained by integrating the EELS intensity over a 50 eV window above the edge onsets for Fe and La, after background removal using a power law. The vertical dotted lines correspond to those on (a).

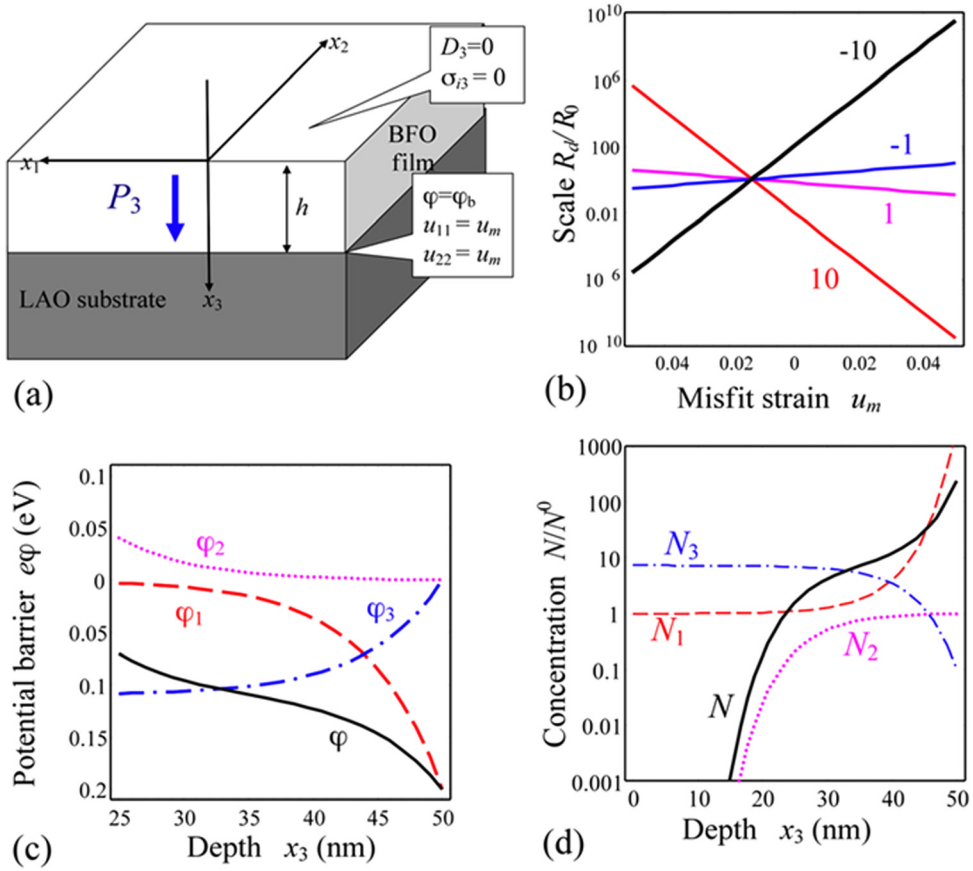

FIG. 4. (a) Schematics of a BFO film clamped on a rigid LAO substrate. Mismatch strain u_m exists at the interface. (b) Dependence of the scale R_d/R_d^0 on the misfit strain u_m calculated for different Vegard coefficients $W = -10, -1, 1, 10 \times 10^{-30}$ m^3 (labels near the curves in 10^{-30} m^3). (c) Potential barrier profiles $e\varphi(x_3)$ (black solid curve) and the individual contributions $\varphi_1(x_3)$ (red dashed line), $\varphi_2(x_3)$ purple dotted line, and $\varphi_3(x_3)$, blue dotted and dashed. The half-film near BFO/LAO interface is shown. The interface is located at 50 nm, while 25 nm refers to the middle region of BFO film. (d) Relative concentration of charged cations $N(x_3)/N^0$ profile (black solid curve) and its contributions: $N_1(x_3)$ red dashed line, $N_2(x_3)$ purple dotted line, and $N_3(x_3)$ blue dotted and dashed. Curves are calculated for BFO film thickness $h = 50$ nm, built-in potential φ_b product on effective charge eZ was taken $eZ\varphi_b = -0.2$ eV, defects equilibrium concentration $N^0 = 10^{24}$ m^{-3}, $W = 1 \times 10^{-30}$ m^3, bulk spontaneous polarization $P_S = 0.9$ C/m, $P_3(0) = -0.5$ C/m, $\varepsilon_{33} \propto 100$, elastic compliances $s_{11} = 5.29 \times 10^{-12}$ Pa^{-1}, $s_{12} = -1.85 \times 10^{-12}$ Pa^{-1}, electrostriction $Q_{11} = 0.032$, $Q_{12} = -0.016$ C^4/m^2; $k_BT = 0.025$ eV at room, $u_m = -0.045$. The interface is located at 50 nm and 0 nm refers to the top of BFO film.

The electric potential can be expressed as $\varphi(x_3) \sim \exp(\pm x_3/R_d)$, where R_d is the Debye screening radius that determines the scale of the potential gradient and the scale of $\delta N(x_3)$ in accordance with Eq. (1). The radius R_d is exponentially dependent on the misfit-related product $W(u_m - Q_{12}P_3^2)$ of Eq. (1) as follows:

$$R_d \cong R_d^0 \exp\left(-\frac{W\left(u_m - Q_{12}\bar{P}_3^2\right)}{2(s_{11}+s_{12})k_BT}\right). \quad (2)$$

The typical values of $R_d^0 = \sqrt{\frac{\varepsilon_0\varepsilon_b k_BT}{2e^2ZN^0}} \sim (1-10)$ nm for the effective charge $Z = 0.1 - 1$, $T = 300$ K, background permittivity[54] $\varepsilon_b \propto 5$ (ε_0 is the dielectric permittivity of vacuum), and defect equilibrium concentration $N^0 = (10^{23} - 10^{24})$ m^{-3}. The absolute values of the strain coefficient (W) for perovskite ABO_3 compounds can be estimated as $|W| \propto$ (0.1–1 nm)^3, at an equilibrium concentration of $N^0 \leq 10^{26}$ m^{-3} (since the concentration of one defect per unit cell with a size ~0.4 nm is about 2.25×10^{28} m^{-3}). The dependence of the scale R_d/R_d^0 on the misfit strain u_m calculated from Eq. (2) for different Vegard coefficients is shown in Figure 4(b). For the moderate Vegard coefficient of ±0.1, the effect of misfit strain is sizeable, leading to a two orders of magnitude change of the Debye screening radius when the misfit changes from −4% to +4%. At higher Vegard coefficients (±1), there is a giant change (of up to six orders of magnitude) in the Debye screening radius with respect to misfit strain. Furthermore, in both cases, there is convergence indicating a minimal or zero screening radius, as the misfit strain is reduced approximately to zero. This result is the direct confirmation of the critical influence of the misfit strain on the screening radius in interfaces comprising ABO_3 perovskites. Considering that, the misfit strain between LAO-BFO interface is ~4.5%, the screening radius is expected to be influenced heavily, thereby affecting the charge equilibrium at the interface, irrespective of the high or moderate Vegard coefficient.

Having clearly established the influence of strain on the LAO-BFO interfacial charge neutrality, the estimation of interfacial potential was carried out. Considering the case of a fixed potential at the BFO/LAO interface $x_3 = h$, $\varphi(h) = \varphi_b$ (φ_b is a built-in potential) and the absence of any electric

displacement normal component D_3 at the BFO/air surface $x_3 = 0$, $D_3 = P_3(0) - \varepsilon_0\varepsilon_{33}\varphi(0)/\partial x_3 = 0$, and the approximate analytical expression can then be derived (see Appendix A of supplementary material for more details)[50] for the electric potential

$$\varphi(x_3) = \varphi_1(x_3) + \varphi_2(x_3) + \varphi_3(x_3), \tag{3a}$$

$$\varphi_1(x_3) = \varphi_b \frac{\cosh(x_3/R_d)}{\cosh(h/R_d)}, \tag{3b}$$

$$\varphi_2(x_3) = -\frac{P_3(0)R_d}{\varepsilon_0\varepsilon_{33}} \frac{\exp((2h - x_3)/R_d) - \exp(x_3/R_d)}{\exp(2h/R_d) + 1}, \tag{3c}$$

$$\varphi_3(x_3) \approx -\frac{R_d^2 eZN^0}{\varepsilon_0\varepsilon_b}\left(1 - \exp\left(\frac{W\left(u_m - Q_{12}\bar{P}_3^2\right)}{(s_{11} + s_{12})k_BT}\right)\right) \times \left(1 - \frac{\cosh(x_3/R_d)}{\cosh(h/R_d)}\right). \tag{3d}$$

Equation (3a) has three contributions to the electric potential inside a BFO film of thickness h. The first contribution, $\varphi_1(x_3)$ given by Eq. (3b), is purely extrinsic and is proportional to the BFO/LAO interface built-in potential φ_b. The second contribution, $\varphi_2(x_3)$ given by Eq. (3c), is proportional to $\sim\frac{P_3}{\varepsilon_0\varepsilon_{33}}$; it originates from the depolarization field[55] in turn caused by the spontaneous and abrupt polarization-breaking at the BFO top surface $x_3 = 0$. The third contribution, $\varphi_3(x_3)$ given by Eq. (3d), follows from the intrinsic screening mechanism of charged defects and the difference between mismatch strain and spontaneous strain $\sim N_m^0\left(u_m - Q_{12}P_S^2\right)$. The contributions to the potential (3a)–(3d) are analyzed in Figure 4(c) for typical BFO and LAO parameters.[56,57] On the x-axis, the LAO-BFO interface is located at 50 nm so that the middle region of the BFO film is located at a position of 25 nm. It can be observed that the contribution from the interface built-in potential $\varphi_1(x_3)$ (red dashed line) drops over two orders of magnitude and reaches a minimum while moving towards the center of the film (25 nm) from the interface (50 nm). The contribution from the intrinsic screening mechanism due to charged defects ($\varphi_3(x_3)$ blue dotted and dashed) changes by one order of magnitude on moving towards the center of the film from the interface. The contribution from the depolarizing field ($\varphi_2(x_3)$ purple dotted line) is relatively small and can be considered insignificant at the LAO-BFO interface, while this becomes a dominating factor at the top end of the BFO film (Figure A, in supplementary information).[50] The combined built-in potential ($e\varphi(x_3)$ black solid line) shows an overall decrease in potential from the LAO-BFO interface towards the center of the film. Thus, results of the modeling relating the influence of misfit strain on the charge equilibrium and the built-in field clearly indicate the existence of substantial built-up potential at the LAO-BFO interface. The critical influence of one on the other can be summarized as follows: the high misfit strain influences the Debye screening radius which, in turn, results in creating built-in potential and charged defects at the LAO-BFO interface. Furthermore, as the misfit strain is relaxed at regions away from the interface both the screening influence and the built-in potential gradually decay.

Similar to the separation of the potential into three contributions, the defects concentration spatial redistribution $N(x_3)$ given by Eq. (1) has three origins, $N_i(x_3) \propto N^0 \exp\left(-\frac{eZ\varphi_i(x_3)}{k_BT}\right)$. The first one originates from the built-in potential at the LAO/BFO interface, $N_1(x_3)$; the second one originates from the depolarization effect, $N_2(x_3)$; and the third one originates from the intrinsic screening mechanism of charged defects $N_3(x_3)$. It is noted that the x_3-independent factor $\exp\left(\frac{W\left(u_m - Q_{12}\bar{P}_3^2\right)}{(s_{11}+s_{12})k_BT}\right)$ in Eq. (1) is not related to defect charge (i.e., it exists for neutral defects also), but this factor cannot lead to cation motion towards the film boundaries. Only charged species can move in accordance with our calculations.

The spatial distribution of charged species is analyzed in Figure 4(d). Along the x-axis, the interface is located at 50 nm, while the top free end of the BFO film is situated at 0 nm. The moderate built-in barrier of $eZ\varphi_b = -0.2$ eV across the LAO-BFO interface results in the charged defects segregating by factors of up to hundreds of times at the interface ($z = h$, $N_1(x_3)$, red dashed line). It should be noted that higher built-in barriers ($eZ\varphi_b \propto -1$ eV) would lead to giant accumulations (more than 10^5 times) that would not be consistent with the Boltzmann approximation used in our model: this case was therefore not considered. The depolarization field can lead to a strong depletion (up to 10^3 times) for a negative sign of $P_3(0)$, at the top surface $z = 0$ ($N_2(x_3)$, purple dotted line). The intrinsic screening mechanism also causes the charged defects to redistribute, but it is essentially weaker than the previous two mechanisms ($N_3(x_3)$, blue dotted and dashed line). The combined charge distribution ($N(x_3)$ black solid line) shows a gradual decay in concentration while moving from the LAO-BFO interface (50 nm) towards the top free end of the film (0 nm). It can therefore be stated that the charged species concentration is maximum at the interface and reduces on moving towards the top of the film. Furthermore, the built-in mechanism can be switched off for the case $\varphi_b = 0$; the depolarization effect can thus be eliminated in the condition $P_3(0) = 0$, while the intrinsic screening mechanism created due to misfit strain remains. Overall, LGD-based theoretical modeling indicates the critical influence of misfit strain on modifying the LAO-BFO interfacial charge equilibrium and the creation of a potential gradient at the interface. Emphatically, it finds this interfacial potential is adequate to generate sufficient flux to result in the intermixing of cations across the interface.

Note that, using Eqs. (1)–(3) for numerical calculations, we used the spontaneous polarization value renormalized by a misfit strain, i.e., from the formulae $\bar{P}_3 = P_S\sqrt{1 - \frac{2Q_{12}u_m}{\alpha(s_{11}+s_{12})}}$, where $P_S = \sqrt{-\frac{\alpha}{\beta}}$ is the "bulk" polarization of the second order ferroelectric in agreement with the Landau model. The high compressive strains (−4.5% in our case) stabilize the out-of-plane polarization,

which are typical for most perovskites. The expression for $\bar{P}_3$ does not account for the structural order parameter that exists in BFO and may lead to the effects described elsewhere.[58] To include the structural subsystem correctly, one must know all of the corresponding expansion coefficients, including the rotostriction tensor and the oxygen octahedral tilt temperature dependence. Unfortunately, all these parameters are not presently available. So, we fit the polarization using "purely ferroelectric" expressions for BFO. Also, we study how sensitive are the contributions to the potential (Eq. (3)) and cations concentration to the polarization $\bar{P}_3$ value. As one can see from Figures 4(c) and 4(d), the main contributions to the electrostatic potential and concentration variation come from the built-in potential (Eq. (3b)) and from the intrinsic screening mechanism of charged defects (Eq. (3d)). Both weakly depend on $\bar{P}_3$. Thus, the temperature variation of the polarization would not substantially affect the cation interdiffusion at the growth temperature.

D. Analysis of Fe EEL spectra-rationalization of theoretical predictions on charged defects

From these theoretical considerations, it is apparent that the presence of charged species at the LAO-BFO interface plays a vital role in neutralizing the potential gradient and in turn acts as a driving force for cation interdiffusion across the interface. In the present LAO-BFO system, the exchange between La and Bi can be considered as charge neutral, since the La charge state is typically fixed as +3 (a +2 oxidation state exists, but is much less stable).[59] Hence, any possible charge imbalance on the BFO side of the interface should manifest itself as a change in the valence state of Fe (possibly accompanied by the creation of oxygen vacancies), which can typically vary from +2 to +3 (although a wider range of oxidation states, −2 to +6, can be observed for Fe). In order to experimentally verify the presence of charged species in the form of Fe valence state change across the LAO-BFO interface, an analysis of the EELS Fe L_3/L_2 intensity ratio was carried out. The observed spectral features in Fe-$L_{2,3}$ EEL spectra arise due to the hybridization between $2p$ and un-occupied d orbitals.[60,61] Any subtle variation of these features is a direct measurement of local electronic structural changes.[62] The L_3/L_2 peak intensity ratio, in particular, was shown to be dependent on the oxidation state of Fe.[63,64] Here, the Fe L_3/L_2 ratio was calculated, in practice, by integrating the positive component of the second derivative of the EEL spectrum at the energy range between 700 and 730 eV,[65,66] using standard functions available in the Digital Micrograph software package.

Figure 5 shows the calculated L_3/L_2 ratio from an EELS linescan acquired across the LAO/BFO interface. It reveals a marked drop at the interface region from a relatively constant value of 5.3 away from the interface (in what could be described as the "bulk" region of the BFO film), which is in good agreement with reported values for Fe3+ compounds. The drop in the interface region convincingly indicates a subtle Fe valence decrease at the interface region,[65] to Fe2.x+, although it is not sufficient to provide a quantitative measure of the exact valence due to the measurement

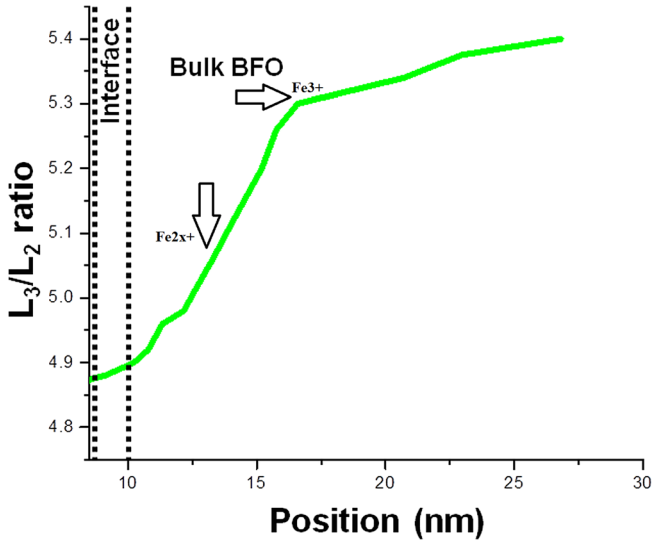

FIG. 5. Profile of the Fe EELS L_3/L_2 ratio across the LAO-BFO interface and into the bulk of the BFO film indicating an apparent change in valence of Fe across an extended region near the interface.

uncertainty. Note that the slight upward slope in the bulk region is likely due to plural scattering effects subtly affecting the edge fine structure analysis, the sample being thicker away from the edge. Nevertheless, it is interesting to note that the L_3/L_2 ratio change occurs across a distance of 6–8 nm, which is wider than the observed chemical interdiffusion profile described in Figure 3, suggesting that the cation migration only partially compensates for the potential gradient and explains why both are observed simultaneously. These extra experimental considerations seem to be in very good agreement with the thermodynamic theory developed above, suggesting that the interfacial strain is high enough to create a potential gradient around the interfacial region, which, in turn, drives cation migration.

IV. DISCUSSION

The misfit strain between LAO and BFO is ∼−4.5%. As stated in the introduction, heteroepitaxial thin films with such massive interfacial strain are expected to relax by the formation of dislocations beyond a critical thickness.[12,67] The critical thickness at which the dislocation formation takes place is inversely related to the lattice mismatch, i.e., the higher the misfit strain between the film and substrate, the lower the thickness for the formation of misfit dislocations.[2,14,36] Furthermore, our MATLAB-based calculation (data not shown) for typical LAO-BFO parameters showed that the critical thickness for the formation of misfit dislocations at the LAO-BFO interface was of the order ∼0.28 nm, which is less than half unit cell. Hence, it appears that other than the formation of dislocations, there exists an underlying mechanism for strain relaxation at the interface. Although, Roytburd *et al.* suggested the R-T phase separation as a primary mechanism for misfit strain relaxation,[17] the present experimental study and the modelling indicate the possibility of misfit strain induced cation diffusion, in addition to phase separation. The RSM data (Figure 1(c)) shows the d value of T-like phase as 0.464 nm and that of R-like phase as

0.416 nm, thereby confirming that BFO film reported here is severely strained, not relaxed.[8,36] It can be stated that despite the phase separation, the film is not completely relaxed. Furthermore, the STEM-HAADF and EELS studies reveal that the interface is physically coherent, but chemically incoherent.

Based on diffusion and thermodynamics theories, the magnitude of the diffusion length scale is influenced by the time and temperature and this applies to all types of interfaces.[68] The cation migration in the oxide heterostructures is expected to be critically influenced by the retention time of the heterostructure at high temperature during fabrication.[42] A similar behaviour is observed in the LAO-BFO interface as well. The parameters, such as flux concentration and diffusion coefficient show a remarkable variation, when time and temperatures are varied (supplementary information, Sec. 2, Figure S1).[50] In addition, the observed cation migration across the LAO-BFO interface is higher than the reported diffusion in Ref. 42. Considering the high temperature stability of LAO, one can expect the high temperature cation migration to be less pronounced. It appears this is not the case. Hence, we strongly believe that in the LAO-BFO system, misfit strain plays a critical role in the observed cation migration.

In order to explain this anomaly, we considered LGD theory and Shenoy formulations and identified three sets of parameter, namely: (a) cation concentration at the interface, (b) the built-up potential, and (c) screening radius (Debye), which can influence the cation inter-diffusion across the LAO-BFO interface. The critical influences of misfit strain on these parameters were considered and the reported values of LAO/BFO system were used for calculations.[56] The combined analysis clearly indicates that misfit strain originated at the ferroelectric film-substrate interface acts as stimulus for strong built-in potential at the region close to the interface and gradually decreases towards the free end of the film. Built-in electric potential leads to the accumulation/ depletion of charged defects at the interface. The corresponding screening potential shows an exponential dependency with misfit strain and shows a gradual decay on moving from the interface towards bulk of the film (Figure 4(c)). The modelling results further confirm that the electrical potential gradient created due to charged defects (cations, vacancies, etc.) can indeed move towards the BFO film boundaries. Furthermore, in order to validate the presence of charged species at the interface, based on the L_3/L_2 EELS intensity ratio,[69] (Figure 5) we make a very subtle claim of this possibility. Overall, the combined influence of misfit strain, inherent charge imbalance at the interface and the bismuth volatility results in creation of charged species/vacancies in the form of Fe with a very slightly modified valence state. Furthermore, the local electronic structure is modified due to volatility of Bi in the form of changes in the Bi-O bond length. Due to this, Fe-O bond length and Fe valance are also expected to be affected. This further leads to charge build-up at interface region. Thus, the experimentally observed cation intermixing over a length scale of ~2 nm can be originated in order to neutralize the built-in field created mainly due to misfit strain. The built-in potential provides the flux for the cation migration.

The peak pair analysis (PPA)[70] (Sec. 3, Figure S2, supplementary information)[50] further confirmed that the film is maximum strained along the direction perpendicular (E_{xx}) to the interface; while the forces required to create dislocations along the interface direction (E_{yy}) are much lower thereby dislocation formation is not kinetically favorable. Thus, the overall misfit strain is compensated by local chemical variation and phase separation of BFO into T and R like phases. The model therefore explains the experimental results qualitatively. This study further confirms that the presence of built-up potential and the corresponding cation diffusion is purely an interfacial phenomenon. These charged defects created by the asymmetrical boundary conditions have a detrimental effect in scaling down the polarization and electromechanical behaviour of strained thin films.[71] It should be noted that in the present study, only the interfacial effects arising due to misfit strain between LAO substrate and BFO film are reported. In any meaningful device architecture based on mixed phase BFO, a bottom electrode, such as lanthanum strontium cobalt oxide (LSCO) or lanthanum nickel oxide (LNO) would be included between the substrate and film.[5,8,9] Thus, the appropriate electrode barrier should not only provide electrical contact but also significantly offset the detrimental effects on the ferroelectric polarization by the potential gradient and diffusion due to misfit strain at the LAO-BFO interface. Overall, in this study, high resolution analytical electron microscopy in combination with LGD theory and Shenoy formulation was used to investigate the misfit strain relaxation mechanism in a highly strained hetero-epitaxial interface. Furthermore, the versatility of high resolution analytical electron microscopy as a tool to resolve the complex interfacial phenomena of the emerging novel functional materials is also demonstrated.

Finally, it is worthwhile to mention that in the present study, only one state of (compressive) misfit strain between the LAO substrate and the BFO film is reported. There are available reports which state that it is possible to strain engineer BFO films with different strain (bulk-like, pure T-like phase) states by fabricating BFO films on varied substrates, such as strontium titanate, $DyScO_3$, and $YAlO_3$.[6,10] Analytical electron microscopy based investigation on the misfit strain relaxation in these BFO thin films can be undertaken as a future work in order to gain a comprehensive understanding on misfit strain relaxation mechanisms in the interfaces comprising the emerging multiferroic oxide. Similarly, in future studies, the factors, such as the influence of the high temperature and time scale on the diffusion kinetics and the process kinetics of PLD can also be included in the modelling as an additional parameter in order to understand the influence between kinetics and strain relaxation mechanisms.

V. CONCLUSIONS

In summary, BFO with mixed R and T phases was fabricated on an LAO substrate using PLD. Atomic resolution images confirmed the formation of a defect free LAO-BFO

interface. Chemical analysis across the interface showed that the LAO-BFO interface was chemically inter-diffused. The Fe from the BFO film and La from substrate inter-mixed over a length scale of ~2–3 nm. LGD theory combined with Stephenson and Highland and Sheldon and Shenoy formalism was used to understand the role of misfit strain to attract charged vacancies to the interfaces. It can be stated that the observed diffusion is essentially due to the presence of an electric potential gradient across the interface. The gradient and strength of the potential are controlled by misfit strain between film and substrate via the Vegard mechanism. It is established that in the LAO-BFO interface, in addition to phase separation of BFO into T and R like phases, potential gradient (created due to interfacial charge imbalances) assisted chemical diffusion acts as a misfit strain relaxation mechanism.

ACKNOWLEDGMENTS

The authors wish to acknowledge Sergei V. Kalinin (ORNL, USA) for stimulating intellectual discussions. P.S.S. thanks Adam Sirokshi (ACMM, University of Sydney) for assistance provided during the cross sectional specimen preparation. P.S.S. and V.N. acknowledge Dr. Reza Mohamood (UNSW, Sydney) for assistance with MATLAB calculations. This work at The University of New South Wales was supported by an ARC Discovery project. The authors acknowledge access to the UNSW node of the Australian Microscopy & Microanalysis Research Facility (AMMRF). A.N.M. and E.A.E. acknowledge State Fund of Fundamental State Fund of Fundamental Research of Ukraine, SFFR-NSF Project No. UU48/002 (associated National Science Foundation Grant No. NSF-DMR-1210588). The SuperSTEM Laboratory is the U.K. Engineering and Physical Science Research Council (EPSRC) national facility of aberration-corrected STEM. The work at National Chiao Tung University is supported by the National Science Council, R.O.C (NSC-101–2119-M-009–003-MY2), Ministry of Education (MOE-ATU 101W961), and Center for interdisciplinary science of National Chiao Tung University.

[1]D. G. Schlom, L.-Q. Chen, C.-B. Eom, K. M. Rabe, S. K. Streiffer, and J.-M. Triscone, Annu. Rev. Mater. Res. **37**, 589 (2007).
[2]K. J. Choi, M. Biegalski, Y. L. Li, A. Sharan, J. Schubert, R. Uecker, P. Reiche, Y. B. Chen, X. Q. Pan, V. Gopalan, L.-Q. Chen, D. G. Schlom, and C. B. Eom, Science **306**, 1005 (2004).
[3]J. H. Haeni, P. Irvin, W. Chang, R. Uecker, P. Reiche, Y. L. Li, S. Choudhury, W. Tian, M. E. Hawley, B. Craigo, A. K. Tagantsev, X. Q. Pan, S. K. Streiffer, L. Q. Chen, S. W. Kirchoefer, J. Levy, and D. G. Schlom, Nature **430**, 758 (2004).
[4]R. J. Zeches, M. D. Rossell, J. X. Zhang, A. J. Hatt, Q. He, C.-H. Yang, A. Kumar, C. H. Wang, A. Melville, C. Adamo, G. Sheng, Y.-H. Chu, J. F. Ihlefeld, R. Erni, C. Ederer, V. Gopalan, L. Q. Chen, D. G. Schlom, N. A. Spaldin, L. W. Martin, and R. Ramesh, Science **326**, 977 (2009).
[5]J. X. Zhang, B. Xiang, Q. He, J. Seidel, R. J. Zeches, P. Yu, S. Y. Yang, C. H. Wang, Y. H. Chu, L. W. Martin, A. M. Minor, and R. Ramesh, Nat. Nanotechnol. **6**, 98 (2011).
[6]Z. Chen, Z. Luo, C. Huang, Y. Qi, P. Yang, L. You, C. Hu, T. Wu, J. Wang, C. Gao, T. Sritharan, and L. Chen, Adv. Funct. Mater. **21**, 133 (2011).
[7]D. Mazumdar, V. Shelke, M. Iliev, S. Jesse, A. Kumar, S. V. Kalinin, A. P. Baddorf, and A. Gupta, Nano Lett. **10**, 2555 (2010).
[8]Q. He, Y. H. Chu, J. T. Heron, S. Y. Yang, W. I. Liang, C. Y. Kuo, H. J. Lin, P. Yu, C. W. Liang, R. J. Zeches, W. C. Kuo, J. Y. Juang, C. T. Chen, E. Arenholz, A. Scholl, and R. Ramesh, Nat. Commun. **2**, 225 (2011).
[9]K.-T. Ko, M. H. Jung, Q. He, J. H. Lee, C. S. Woo, K. Chu, J. Seidel, B.-G. Jeon, Y. S. Oh, K. H. Kim, W.-I. Liang, H.-J. Chen, Y.-H. Chu, Y. H. Jeong, R. Ramesh, J.-H. Park, and C.-H. Yang, Nat. Commun. **2**, 567 (2011).
[10]J. X. Zhang, Q. He, M. Trassin, W. Luo, D. Yi, M. D. Rossell, P. Yu, L. You, C. H. Wang, C. Y. Kuo, J. T. Heron, Z. Hu, R. J. Zeches, H. J. Lin, A. Tanaka, C. T. Chen, L. H. Tjeng, Y. H. Chu, and R. Ramesh, Phys. Rev. Lett. **107**, 147602 (2011).
[11]J. W. Matthews, J. Vac. Sci. Technol. (N. Y., NY, U. S.) **12**, 126 (1975).
[12]J. S. Speck and W. Pompe, J. Appl. Phys. **76**, 466 (1994).
[13]S. S. Iyer and F. K. LeGoues, J. Appl. Phys. **65**, 4693 (1989).
[14]W. Nix, Metall. Mater. Trans. A **20**, 2217 (1989).
[15]M. F. Chisholm and S. J. Pennycook, Philos. Mag. **86**, 4699 (2006).
[16]Y. Qi, C. Huang, Z. Chen, Z. Luo, Y. Wang, J. Guo, T. White, J. Wang, C. Gao, T. Sritharan, and L. Chen, Appl. Phys. Lett. **99**, 132905 (2011).
[17]A. L. Roytburd, J. Ouyang, B. M. Boyerinas, and H. A. Bruck, Appl. Phys. Lett. **99**, 172902 (2011).
[18]M. Arredondo, Q. M. Ramasse, M. Weyland, R. Mahjoub, I. Vrejoiu, D. Hesse, N. D. Browning, M. Alexe, P. Munroe, and V. Nagarajan, Adv. Mater. (Weinheim, Ger.) **22**, 2430 (2010).
[19]N. Nakagawa, H. Y. Hwang, and D. A. Muller, Nature Mater. **5**, 204 (2006).
[20]J. L. MacManus-Driscoll, P. Zerrer, H. Wang, H. Yang, J. Yoon, A. Fouchet, R. Yu, M. G. Blamire, and Q. Jia, Nature Mater. **7**, 314 (2008).
[21]A. Lubk, M. D. Rossell, J. Seidel, Y. H. Chu, R. Ramesh, M. J. Hÿtch, and E. Snoeck, Nano Lett. **13**, 1410 (2013).
[22]A. Brinkman, M. Huijben, M. van Zalk, J. Huijben, U. Zeitler, J. C. Maan, W. G. van der Wiel, G. Rijnders, D. H. A. Blank, and H. Hilgenkamp, Nature Mater. **6**, 493 (2007).
[23]P. Yu, W. Luo, D. Yi, J. X. Zhang, M. D. Rossell, C.-H. Yang, L. You, G. Singh-Bhalla, S. Y. Yang, Q. He, Q. M. Ramasse, R. Erni, L. W. Martin, Y. H. Chu, S. T. Pantelides, S. J. Pennycook, and R. Ramesh, Proc. Natl. Acad. Sci. U.S.A. **109**, 9710 (2012).
[24]S. A. Chambers, M. H. Engelhard, V. Shutthanandan, Z. Zhu, T. C. Droubay, L. Qiao, P. V. Sushko, T. Feng, H. D. Lee, T. Gustafsson, E. Garfunkel, A. B. Shah, J. M. Zuo, and Q. M. Ramasse, Surf. Sci. Rep. **65**, 317 (2010).
[25]J. He, A. Borisevich, S. V. Kalinin, S. J. Pennycook, and S. T. Pantelides, Phys. Rev. Lett. **105**, 227203 (2010).
[26]A. Borisevich, O. S. Ovchinnikov, H. J. Chang, M. P. Oxley, P. Yu, J. Seidel, E. A. Eliseev, A. N. Morozovska, R. Ramesh, S. J. Pennycook, and S. V. Kalinin, ACS Nano **4**, 6071 (2010).
[27]P. Yu *et al.*, Phys. Rev. Lett. **105**, 027201 (2010).
[28]B. W. Sheldon and V. B. Shenoy, Phys. Rev. Lett. **106**, 216104 (2011).
[29]J. Chakhalian, J. W. Freeland, G. Srajer, J. Strempfer, G. Khaliullin, J. C. Cezar, T. Charlton, R. Dalgliesh, C. Bernhard, G. Cristiani, H. U. Habermeier, and B. Keimer, Nat. Phys. **2**, 244 (2006).
[30]S. M. Wu, S. A. Cybart, P. Yu, M. D. Rossell, J. X. Zhang, R. Ramesh, and R. C. Dynes, Nature Mater. **9**, 756 (2010).
[31]A. Y. Borisevich, A. N. Morozovska, Y.-M. Kim, D. Leonard, M. P. Oxley, M. D. Biegalski, E. A. Eliseev, and S. V. Kalinin, Phys. Rev. Lett. **109**, 065702 (2012).
[32]D. B. Williams and C. B. Carter, *Transmission Electron Microscopy—A Textbook for Materials Science* (Springer Science + Business Media, 2009).
[33]Z. Chen, L. You, C. Huang, Y. Qi, J. Wang, T. Sritharan, and L. Chen, Appl. Phys. Lett. **96**, 252903 (2010).
[34]C. W. Huang, Y. H. Chu, Z. H. Chen, J. Wang, T. Sritharan, Q. He, R. Ramesh, and L. Chen, Appl. Phys. Lett. **97**, 152901 (2010).
[35]H. Béa, B. Dupé, S. Fusil, R. Mattana, E. Jacquet, B. Warot-Fonrose, F. Wilhelm, A. Rogalev, S. Petit, V. Cros, A. Anane, F. Petroff, K. Bouzehouane, G. Geneste, B. Dkhil, S. Lisenkov, I. Ponomareva, L. Bellaiche, M. Bibes, and A. Barthélémy, Phys. Rev. Lett. **102**, 217603 (2009).
[36]A. R. Damodaran, S. Lee, J. Karthik, S. MacLaren, and L. W. Martin, Phys. Rev. B **85**, 024113 (2012).
[37]A. T. Fiory, J. C. Bean, L. C. Feldman, and I. K. Robinson, J. Appl. Phys. **56**, 1227 (1984).
[38]S. J. Pennycook and D. E. Jesson, Phys. Rev. Lett. **64**, 938 (1990).
[39]P. Hartel, H. Rose, and C. Dinges, Ultramicroscopy **63**, 93 (1996).
[40]S. J. Pennycook and D. E. Jesson, Ultramicroscopy **37**, 14 (1991).

[41]D. O. Klenov and S. Stemmer, Ultramicroscopy **106**, 889 (2006).
[42]P. S. S. R. Krishnan, Q. M. Ramasse, W.-I. Liang, Y.-H. Chu, V. Nagarajan, and P. Munroe, J. Appl. Phys. **112**, 104102 (2012).
[43]L. J. Allen, S. D. Findlay, A. R. Lupini, M. P. Oxley, and S. J. Pennycook, Phys. Rev. Lett. **91**, 105503 (2003).
[44]P. Wang, A. J. D'Alfonso, S. D. Findlay, L. J. Allen, and A. L. Bleloch, Phys. Rev. Lett. **101**, 236102 (2008).
[45]A. B. Shah, Q. M. Ramasse, X. Zhai, J. G. Wen, S. J. May, I. Petrov, A. Bhattacharya, P. Abbamonte, J. N. Eckstein, and J.-M. Zuo, Adv. Mater. (Weinheim, Ger.) **22**, 1156 (2010).
[46]P. S. S. R. Krishnan, M. Arredondo, M. Saunders, Q. M. Ramasse, N. Valanoor, and P. Munroe, J. Appl. Phys. **109**, 034103 (2011).
[47]E. Detemple, Q. M. Ramasse, W. Sigle, G. Cristiani, H. U. Habermeier, B. Keimer, and P. A. van Aken, J. Appl. Phys. **112**, 013509 (2012).
[48]A. N. Morozovska, E. A. Eliseev, G. S. Svechnikov, and S. V. Kalinin, Phys. Rev. B **84**, 045402 (2011).
[49]G. B. Stephenson and M. J. Highland, Phys. Rev. B **84**, 064107 (2011).
[50]See supplementary material at http://dx.doi.org/10.1063/1.4862556 for a detailed calculations and Figure A for potential distribution. The diffusion profile of LAO-BFO interface given in Figure S1. The strain analysis by peak pair analysis is given in Figure S2.
[51]Y.-T. Cheng and M. W. Verbrugge, J. Power Sources **190**, 453 (2009).
[52]X. Zhang, A. M. Sastry, and W. Shyy, J. Electrochem. Soc. **155**, A542 (2008).
[53]D. A. Freedman, D. Roundy, and T. A. Arias, Phys. Rev. B **80**, 064108 (2009).
[54]A. K. Tagantsev and G. Gerra, J. Appl. Phys. **100**, 051607 (2006).
[55]E. Eliseev and A. Morozovska, J. Mater. Sci. **44**, 5149 (2009).
[56]G. Catalan and J. F. Scott, Adv. Mater. (Weinheim, Ger.) **21**, 2463 (2009).
[57]J. X. Zhang, Y. L. Li, Y. Wang, Z. K. Liu, L. Q. Chen, Y. H. Chu, F. Zavaliche, and R. Ramesh, J. Appl. Phys. **101**, 114105 (2007).
[58]I. C. Infante, S. Lisenkov, B. Dupé, M. Bibes, S. Fusil, E. Jacquet, G. Geneste, S. Petit, A. Courtial, J. Juraszek, L. Bellaiche, A. Barthélémy, and B. Dkhil, Phys. Rev. Lett. **105**, 057601 (2010).
[59]P. Patnaik, *Handbook of Inorganic Chemical Compounds* (McGraw-Hill, 2003).
[60]R. D. Leapman, L. A. Grunes, and P. L. Fejes, Phys. Rev. B **26**, 614 (1982).
[61]C. Colliex, T. Manoubi, and C. Ortiz, Phys. Rev. B **44**, 11402 (1991).
[62]R. D. Leapman and L. A. Grunes, Phys. Rev. Lett. **45**, 397 (1980).
[63]J. H. Paterson and O. L. Krivanek, Ultramicroscopy **32**, 319 (1990).
[64]H. K. Schmid and W. Mader, Micron **37**, 426 (2006).
[65]F. Cosandey, D. Su, M. Sina, N. Pereira, and G. G. Amatucci, Micron **43**, 22 (2012).
[66]P. A. van Aken and B. Liebscher, Phys. Chem. Miner. **29**, 188 (2002).
[67]J. W. Matthews, S. Mader, and T. B. Light, J. Appl. Phys. **41**, 3800 (1970).
[68]P. G. Shewmom, *Diffusion in Solids* (Mc-Graw Hill, New York, 1989).
[69]P. A. van Aken, B. Liebscher, and V. J. Styrsa, Phys. Chem. Miner. **25**, 323 (1998).
[70]P. L. Galindo, S. Kret, A. M. Sanchez, J.-Y. Laval, A. Yáñez, J. Pizarro, E. Guerrero, T. Ben, and S. I. Molina, Ultramicroscopy **107**, 1186 (2007).
[71]C. Duan, F. S. Renat, N. M. Wei, S. J. Sitaram, and E. Y. Tsymbal, Nano Lett. **6**, 483 (2006).